# On Comprehensive Description and Analysis of MMC Control Design: Simulation and Experimental Study

Haibo Zhang, Mohamed Moez Belhaouane, Frédéric Colas, Riad Kadri, François Gruson and Xavier Guillaud, *Member, IEEE*

***Abstract*—This paper presents an evolution of control systems of Modular Multilevel Converters (MMCs) focusing on the internal voltages and currents dynamics. MMCs have passive components inside the converter that create extra dynamics compared to conventional VSCs. Some control schemes that do not consider these internal dynamics may still stabilize the system asymptotically thanks to the linearisation in the modulation step. However these control schemes are less robust because they are prone to poor damped oscillations on the dc side of the converter. The MMC circuit and energy relationships are presented in this paper. Along with a gradual development of the energy based control, the important roles of each internal dynamics are clearly demonstrated. Experimental results are presented to show the impacts of the linearisation in the modulation step on the system behaviour.**

***Index Terms*—Modular Multilevel Converter (MMC), Energy Based Control, Modulation Methods.**

## I. Introduction

Modular Multilevel Converter (MMC) has been introduced in [1] and first used for HVDC power conversion in the Trans Bay Cable project in 2010 [2]. Its modular design brings several advantages such as lower switching losses, lower harmonic contents in the output ac voltage and smaller station footprint. These advantages make it potential for applications of wide voltage range.

A variety of studies have covered the design, modelling, operation and control of MMCs. This converter exhibits clear differences compared to conventional VSCs mainly because of the presence of passive components inside converters, i.e., the capacitor in each submodule (SM) and the inductance in each arm. This means that MMCs possess additional internal dynamics, namely the SM capacitor voltages and the differential currents.

Early analysis and controls of the MMC are based on the Direct Modulation [3], where the internal dynamics are not controlled. It had been a long time that the stability of the internal dynamics was not examined, until a convergence analysis was shown in [4] and a more rigorous proof by Lyapunov's stability criteria was provided in [5]. It is demonstrated that the system is asymptotically stable. The modulation stage does not compensate the voltage ripples due to charging and discharging of the arm capacitor, therefore resulting in insertion index errors. These errors force the arm capacitor voltages to converge to the dc link voltage. An issue of such control is the appearance of large second-order harmonics in the differential currents that increase the RMS value of the internal currents and therefore the power losses. Attempts to suppress the oscillations includes using resonant controllers [6], and more commonly, applying a Circulating Current Suppression Controller (CCSC) to inject harmonics into the differential current [7]. However, recent studies have reported that MMCs controlled with CCSC are prone to poorly damped oscillations or even instability [8], [9]. Participation factor analysis in [10] has identified that these oscillations originate from the uncontrolled dc link current and the MMC stored energy.

Therefore, it is required to control the MMC internal dynamics. Dealing with the stored energy in the MMC, these controls are often called energy based control. The first work of such kind of control is introduced in [11]. It proposes that one controller regulate the sum of the upper and lower arms energy, and one controller regulate the difference between them. There is no differential current control loop in its control scheme. Energy balancing with all state variables regulated are developed in [12], [13] using cascaded controllers. Two independent currents, the differential current and the grid current are considered as inner loops. A similar cascaded control principle while using the decoupled double synchronous reference frame (DDSRF) is developed in [14]. Variables are separately controlled according to their sequence and harmonic order. In energy based control, the differential currents play an important role in power transfer between dc and ac sides and energy balancing between upper and lower arms. An in-depth description of these internal dynamics is given in this paper.

Although the modulation is commonly linearised with a constant voltage, MMCs can also be modulated with measured arm capacitor voltages containing ripples. In this paper, impacts of linearisation at the modulation stage are demonstrated in the simulation and experimental tests. Based on these results, the authors suggest that the modulation method be

This research work has been supported by RTE, the French TSO and ENR_Trans1 17007725, project funded by the FEDER European Union project.

Haibo Zhang, Mohamed Moez Belhaouane, Xavier Guillaud are with Univ. Lille, Arts et Metiers Institute of Technology, Centrale Lille, HEI, ULR 2697 - L2EP - Laboratoire d'Electrotechnique et d'Electronique de Puissance, F-59000 Lille, France (e-mail: haibo.zhang@centralelille.fr, mohamed-moez.belhaouane@centralelille.fr, xavier.guillaud@centralelille.fr).

Frédéric Colas, Riad Kadri, François Gruson are with Arts et Metiers Institute of Technology, Univ. Lille, Centrale Lille, HEI, HESAM Université, EA 2697 - L2EP - Laboratoire d'Electrotechnique et d'Electronique de Puissance, F-59000 Lille, France (e-mail: Frederic.colas@ensam.eu, riad.kadri@ensam.eu, francois.gruson@ensam.eu).

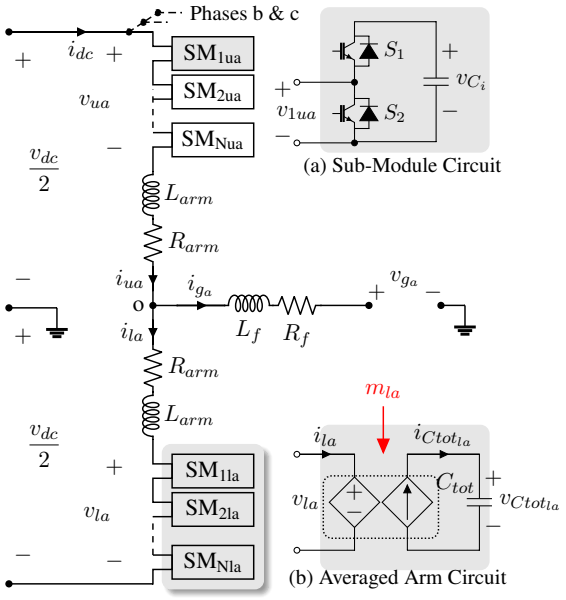


Fig. 1. Grid connected MMC circuit diagram

chosen before developing the MMC control system.

In this paper, rigorous relationships of the MMC circuit and energy dynamics are established in Section II. Differences of two modulation methods, compensating or not compensating the arm capacitor voltage ripples, are shown in Section III. Based on Section II and III, Section IV gives a progressive development of the energy based control. The role of each dynamics are demonstrated in the simulation results. Experimental tests using a scaled-down grid-connected MMC prototype are performed in Section V.

## II. MMC VARIABLES AND MODELLING

The circuit representation of the MMC is shown in Fig. 1. There is one leg for each phase *a*, *b*, *c* and each consists of an upper and a lower arm. The arm includes $N$ series connected SMs, an arm inductor $L_{arm}$ (with internal resistance $R_{arm}$) offers dc fault current limitation. An SM with half-bridge topology is depicted in Fig. 1(a). Neglecting the voltage drop on the inductor and resistor, at every time instant, the arm voltage $v_{ulj}$ equals to the sum of all inserted SMs voltages. If it is assumed that all the SM capacitors voltages are maintained in a close range, the entire SM string can be replaced by an equivalent one $C_{tot}$, leading to the Arm Averaged Model (AAM) shown in Fig. 1(b). $L_f$ and $R_f$ are the transformer's impedance.

### A. AAM circuit relationship

In the averaged arm circuit, $m$ is a continuous insertion index. The equivalent capacitor voltage $v_{Ctot}$ and current $i_{Ctot}$ in each arm has the following relationship:

$$v_{ulj} = m_{ulj} v_{Ctot_{ulj}} \qquad i_{Ctot_{ulj}} = m_{ulj} i_{ulj} \tag{1}$$

$$i_{Ctot_{ulj}} = C_{tot} \frac{dv_{Ctot_{ulj}}}{dt} \tag{2}$$

Subscript $j$ denotes each phase $a$, $b$, $c$. Subscripts $u$ and $l$ represent upper and lower arms, respectively. We can obtain the following circuit relationships by applying the Kirchhoff's voltage law on each phase of the MMC:

$$\frac{v_{dc}}{2} = v_{uj} + L_{arm}\frac{di_{uj}}{dt} + R_{arm} i_{uj} + L_f \frac{di_{g_j}}{dt} + R_g i_{g_j} + v_{g_j} \tag{3}$$

$$\frac{v_{dc}}{2} = v_{lj} + L_{arm}\frac{di_{lj}}{dt} + R_{arm} i_{lj} - L_f \frac{di_{g_j}}{dt} - R_g i_{g_j} - v_{g_j} \tag{4}$$

where $v_g$ is the voltage at Point of Common Coupling (PCC) and $i_g$ is the grid current. The addition of (3) and (4) yields the dc part of the AAM:

$$\frac{v_{dc}}{2} - v_{diff_j} = L_{arm}\frac{di_{diff_j}}{dt} + R_{arm} i_{diff_j} \tag{5}$$

where the differential voltage $v_{diff}$ is an internal voltage that drives the differential current $i_{diff}$. They are defined as:

$$v_{diff_j} \triangleq \frac{v_{uj} + v_{lj}}{2} \;;\; i_{diff_j} \triangleq \frac{i_{uj} + i_{lj}}{2} \tag{6}$$

In the same fashion, the subtraction of (3) and (4) yields an ac part of the AAM:

$$v_{v_j} - v_{g_j} = L_{eq}\frac{di_{g_j}}{dt} + R_{eq} i_{g_j} \tag{7}$$

where $L_{eq} = L_f + {}^{L_{arm}}/_{2}$, and the voltage $v_v$ is an internal voltage that drives the grid current $i_g$. They are defined as:

$$v_{v_j} \triangleq \frac{v_{lj} - v_{uj}}{2} \;;\; i_{g_j} = i_{uj} - i_{lj} \tag{8}$$

### B. Energy relationship

A model linking the average level of the stored energy on a grid period and the currents is proposed. It will be used to design the control structures.

The energy stored in the MMC arms is associated with the voltage of its equivalent arm capacitor:

$$W_{ulj} = \frac{1}{2} C_{tot} v^2_{Ctot_{ulj}} \tag{9}$$

Hereinafter, energy sum $W^{\Sigma}$ stands for the sum of energy stored in the upper and lower arms in one leg; energy difference $W^{\Delta}$ stands for the difference between them:

$$W^{\Sigma}_j = \frac{1}{2} C_{tot}\left(v^2_{Ctot_{uj}} + v^2_{Ctot_{lj}}\right) \tag{10}$$

$$W^{\Delta}_j = \frac{1}{2} C_{tot}\left(v^2_{Ctot_{uj}} - v^2_{Ctot_{lj}}\right) \tag{11}$$

The energy sum $W^{\Sigma}_j$ oscillates mainly at twice the grid frequency negative sequence $-2\omega_g$ [14], and its average value on a grid period is noted as $\overline{W}^{\Sigma}_j$. Similarly, it is found that the energy difference $W^{\Delta}_j$ oscillates mainly at the grid frequency $\omega_g$, and its average value on a grid period is noted as $\overline{W}^{\Delta}_j$.

Neglecting the losses in the MMC, the time derivative of the energy sum and the powers in the dc and ac grids must have the following relationship at any time instant [15]:

$$\frac{dW^{\Sigma}_j}{dt} \approx p_{dc_j} - p_{ac_j} \tag{12}$$

$$= v_{dc} i_{diff_j} - p_{ac_j} \tag{13}$$

where $p_{dc_j}$ and $p_{ac_j}$ are the power at the dc and ac parts of one phase. The differential current can be split into a dc part and an ac part [13]. During one grid period of a balanced grid, the variation of the average energy sum is only determined by the dc component of the differential current:

$$\frac{d\overline{W}_j^{\Sigma}}{dt} \approx v_{dc} i_{diff_j}^{dc} - \frac{1}{3} P_{ac}^* \tag{14}$$

where $P_{ac}^*$ is the total ac power of the three phases, $i_{diff_j}^{dc}$ is the dc component of the differential current. A further assumption of $P_{ac} \approx P_{ac}^*$ is made in this equation.

The time derivative of the energy difference is

$$\frac{dW_j^{\Delta}}{dt} = v_{uj} i_{uj} - v_{lj} i_{lj} \tag{15}$$

$$= v_{diff_j} i_{g_j} - 2 v_{v_j} i_{diff_j} \tag{16}$$

In steady state, $v_{diff_j} \approx {}^{v_{dc}}/_{2}$, the first product at the right side of (16) has a relatively small effect on the variation of $W_j^{\Delta}$ [11]. In the second product, $v_{v_j}$ could be approximated to the ac grid voltage $v_{g_j}$ because normally $L_{eq}$ is relatively small. Therefore:

$$\begin{bmatrix} v_{v_a} \\ v_{v_b} \\ v_{v_c} \end{bmatrix} \approx \sqrt{2} V_g \begin{bmatrix} \cos(\omega_g t) \\ \cos(\omega_g t - \frac{2\pi}{3}) \\ \cos(\omega_g t + \frac{2\pi}{3}) \end{bmatrix} \tag{17}$$

It can be noticed that $v_{v_j}$ is sinusoidal with fundamental frequency and its average is zero. In order to have a dc component in the product of two sinusoidal signals, these two signals must have components of the same frequency. As a result, only the fundamental frequency component determinates the variation of $W_j^{\Delta}$. The fundamental frequency component of differential current is denoted as $i_{diff_j}^{ac}$:

$$\begin{bmatrix} i_{diff_a}^{ac} \\ i_{diff_b}^{ac} \\ i_{diff_c}^{ac} \end{bmatrix} = \sqrt{2} \begin{bmatrix} I_{diff_a}^{ac} \cos(\omega_g t + \varphi_a) \\ I_{diff_b}^{ac} \cos(\omega_g t - \frac{2\pi}{3} + \varphi_b) \\ I_{diff_c}^{ac} \cos(\omega_g t + \frac{2\pi}{3} + \varphi_c) \end{bmatrix} \tag{18}$$

where $I_{diff_j}^{ac}$ is the RMS value of the fundamental frequency component the differential current per phase. $\varphi_j$ is its phase angle. Substituting (17) and (18) into (16), we can find the only non-zero component determining the variation of the energy difference is

$$\frac{dW_j^{\Delta}}{dt} \approx -2 V_g I_{diff_j}^{ac} \cos\varphi_j \tag{19}$$

The phase angle of the fundamental frequency component of the differential current $\varphi_j$ may differ in each phase.

## III. Modulation methods

### A. Arm voltage reference generation

Whatever kind of control structure is used, a set of voltage references of $v_{v_j}^*$ and $v_{diff_j}^*$ will be generate to meet corresponding control requirements. Then, we can obtain the upper and lower arm voltage references via (6) and (8):

$$v_{uj}^* = v_{diff_j}^* - v_{v_j}^* \tag{20}$$

$$v_{lj}^* = v_{diff_j}^* + v_{v_j}^* \tag{21}$$

### B. Modulation and insertion index generation

The insertion index $m$ is generated by substituting (20) and (21) into (1):

$$m_{uj}^* = \frac{v_{uj}^*}{v_{Ctot_{uj}}} \; ; \; m_{lj}^* = \frac{v_{lj}^*}{v_{Ctot_{lj}}} \tag{22}$$

where $v_{Ctot_{ulj}}$ is the actual measurement from the MMC arms. As indicated in (2), it contains oscillating components due to the charging and discharging of the finite-value arm capacitor $C_{tot}$. This modulation index calculation method considering the oscillating components of $v_{Ctot_{ulj}}$ is named as *Compensated modulation* (CM) method. A linearised alternative which approximates $v_{Ctot_{ulj}}$ to its dc component $v_{dc}$, is named as *Uncompensated modulation* (UCM).

$$m_{uj}^* = \frac{v_{uj}^*}{v_{dc}} \; ; \; m_{lj}^* = \frac{v_{lj}^*}{v_{dc}} \tag{23}$$

where $v_{dc}$ can be chosen as a fixed value or an actual measurement of the dc link voltage. The later one is preferred because the dc component is not constant in cases that the MMC is not connected to a stiff dc source [15]. Also, the measured value provides slightly improved stability [16].

The fact of whether to consider the oscillating component in the insertion index generation results in different behaviours on $i_{diff_j}$ and the system asymptotic stability [4]. With the chosen modulation method, control structures can be derived to generate the voltage reference $v_{diff_j}^*$ which satisfies certain requirements on the dynamics.

A series of the combination of the modulation methods and the control structures are shown in Fig. 2. To clearly show the impacts of the modulation methods on the MMC system behaviour, a progressive increment of the internal dynamics control structure are shown in the next section.

## IV. Control structures

The studied converter is connected to a dc source as shown in Fig. 2. The ac side is controlled to follow a given power reference. It has been recalled that the differential current and the grid current are decoupled in (5) and (7). Therefore, any grid current control technique can be applied with no impact on the differential current. In this paper, a classical grid current control in dq reference frame is used. Apply the Park's transformation on (7), the ac currents regulation can be realised by manipulating $v_{v_{dq}}^*$ via two PI controllers $\text{PI}_{i_{gdq}}$ in the $dq$ frame.

$$v_{v_d}^* = \text{PI}_{i_{gd}}(i_{g_d}^* - i_{g_d}) + v_{g_d} - \omega_g L_{eq} i_{g_q} \tag{24}$$

$$v_{v_q}^* = \text{PI}_{i_{gq}}(i_{g_q}^* - i_{g_q}) + v_{g_q} + \omega_g L_{eq} i_{g_d} \tag{25}$$

Apply the inverse Park's transformation, we obtain three sinusoidal reference signals $v_{v_j}^*$. Then the rest of this section will focus on the control structures of the dc part of the MMC, the arm capacitor voltages and the differential currents.

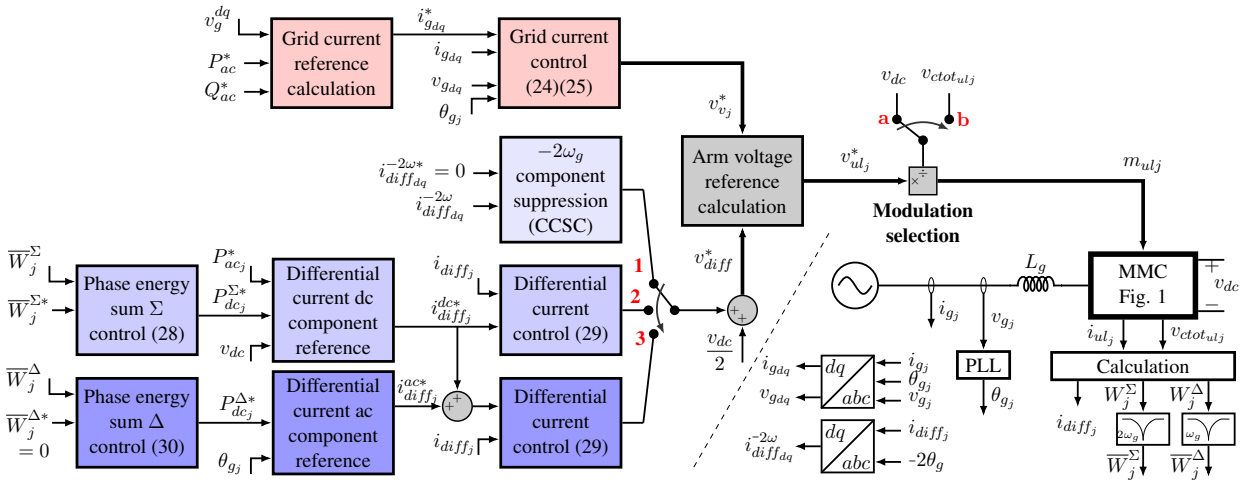


Fig. 2. Control structures of the MMC

### A. UCM and Non Energy Balancing Control (**a1**)

From Fig. 2, by switching the modulation to position **a** and send $v_{dc}/2$ to $v^*_{diff}$, the insertion indices are calculated with *Direct Modulation*. It is the simplest form of the *Uncompensated Modulation* (UCM). The upper and lower arm voltage references are generated by using two complementary sinusoidal signals:

$$v^*_{uj} = \frac{v_{dc}}{2} - v^*_{v_j} \tag{26}$$

$$v^*_{lj} = \frac{v_{dc}}{2} + v^*_{v_j} \tag{27}$$

UCM enables the six arm equivalent capacitor voltages $v_{Ctot}$ to converge naturally towards the dc bus voltage $v_{dc}$ [4]. Although the system is asymptotically stable. the uncontrolled differential current contains a great negative second harmonic circulating component that increases the converter losses. Thus, the Circulating Current Suppression Controller (CCSC) is usually adopted to eliminate this circulating current [17]. This additional control at position **1** in the Fig. 2 is developed under the double line-frequency, negative-sequence rotational frame. Fig. 3 shows the simulation result of the MMC controlled by CCSC. The upper and lower arm capacitor voltages are around 1 pu ($V_{dc}$). However, the power step at 0.1 s induces a great oscillation on the dc current. Through participation factor analysis in [10], the appearance of this poorly damped oscillation is due to the interaction between the dc bus voltage and the internal stored energy of the MMC. To avoid that, the dc link current should be controlled. This is solved by regulating the stored energy per leg in the next control structure **a2**.

### B. UCM and Horizontal Energy Balancing Control (**a2**)

Through (13) and (14), the average energy stored in the MMC legs can be controlled by manipulating the dc components of the differential currents. The references of the differential currents $i^{dc*}_{diff_j}$ can be generated as:

$$i^{dc*}_{diff_j} = \frac{1}{v_{dc}}\left(\mathrm{PI}_{W^\Sigma_j}\left(\overline{W}^{\Sigma*}_j - \overline{W}^{\Sigma}_j\right) + \frac{1}{3}P^*_{ac}\right) \tag{28}$$

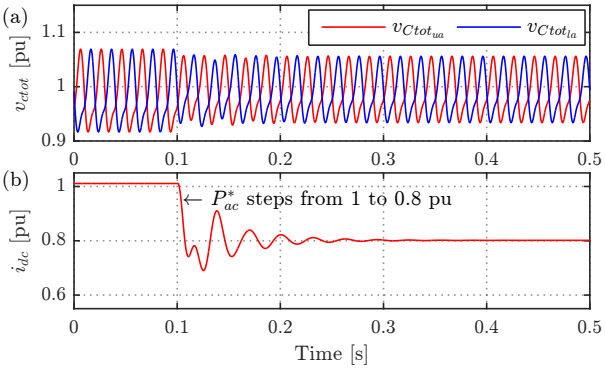


Fig. 3. Simulation results of Control Structure **a1**: (a) arm capacitor voltages $v_{Ctot_{ula}}$; (b) dc current $i_{dc}$.

where $\mathrm{PI}_{W^\Sigma_j}$ is the PI controller for sum energy regulation. The average value of the energy sum can be obtained with a second-order notch filter tuned at $2\omega_g$ [18]. Since the double frequency components only circulate inside the MMC legs [17], the sum of the dc components of the differential currents makes up the dc current. A cascade PI controller $\mathrm{PI}_{i_{diff_j}}$ is used to control $i^{dc}_{diff_j}$ by manipulating $v^*_{diff_j}$:

$$v^*_{diff_j} = \mathrm{PI}_{i_{diff_j}}(i^*_{diff_j} - i_{diff_j}) \tag{29}$$

Fig. 4 shows the simulation results of Control Structure **a2**. At 0.1 s, the ac power reference steps from 1 to 0.8 pu, the dc current has a much higher damping than that in Control Structure **a1**. The energy sum in each leg is controlled to follow its reference at 0.3 s. Both upper and lower voltages are around 1 pu, which means the energy difference between the upper and lower legs, though no explicit control applied, is expected to be 0 due to the convergence of UCM.

However, there is a priority order between the applied total energy control dynamic and the natural convergence rate of the UCM. The applied control dynamic must be slower in order to avoid a dynamic interaction between energy balancing of two upper and lower arms. The convergence rate can only be approximately quantified depending on the MMC parameters.

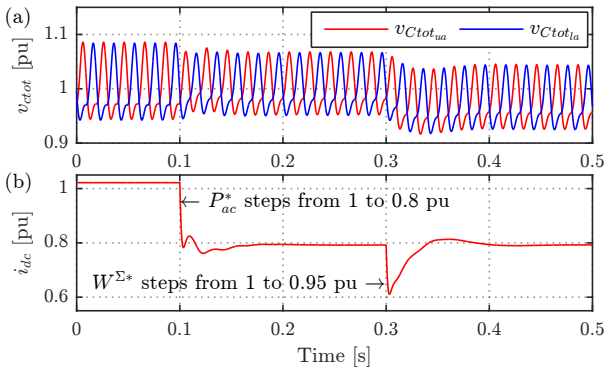


Fig. 4. Simulation results of Control Structure **a2**. (a) arm capacitor voltages $v_{Ctot_{ula}}$; (b) dc current $i_{dc}$.

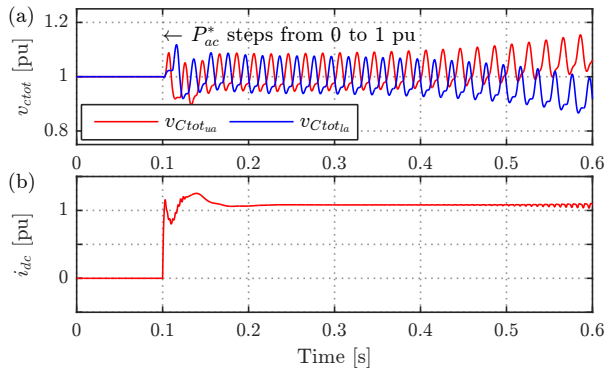


Fig. 5. Simulation results of the Control Structure **a2** with a fast controller dynamic, arm capacitor voltages $v_{Ctot_{ula}}$ diverge from $V_{dc}$.

For a MMC with parameters shown in Table I, the convergence rate is of tens of milliseconds. Fig. 5 shows that the arm capacitor voltages diverge when the applied controller $C_{i_{diff_j}}$ has a high bandwidth. In this figure, the sum of the upper and lower arm voltages stays at 1 pu, while the difference between them keeps increasing. This interaction between the applied total energy dynamic and the natural convergence rate of the UCM compromises the robustness of this method.

Two solutions can be used to avoid this interaction. First solution is to abandon the natural convergence property of UCM by switching the modulation selection to CM at position **b**. The MMC is now controlled with Control Structure **b2** in Fig. 2, however, only energy sum is guaranteed in this structure. The second solution is to decouple these two dynamics by adding an additional control loop for the energy difference. This is shown in the next control structure.

### C. UCM and Vertical Energy Balancing Control (*a3*)

To avoid the issue of the interference between the energy sum control and the slow convergence rate of the UCM, the solution is to eliminate the energy difference with an explicit control loop. According to (19), the variation of the energy difference can be influenced by two elements: 1) the rms value of the fundamental frequency component of differential current $I^{ac}_{diff_j}$, and 2) its phase angles $\varphi_j$.

The selection of $\varphi_j$ has a large flexibility. As long as $\cos\varphi_j > 0$, a PI controller $\mathrm{PI}_{W^{\Delta}_j}$ can be used for generating

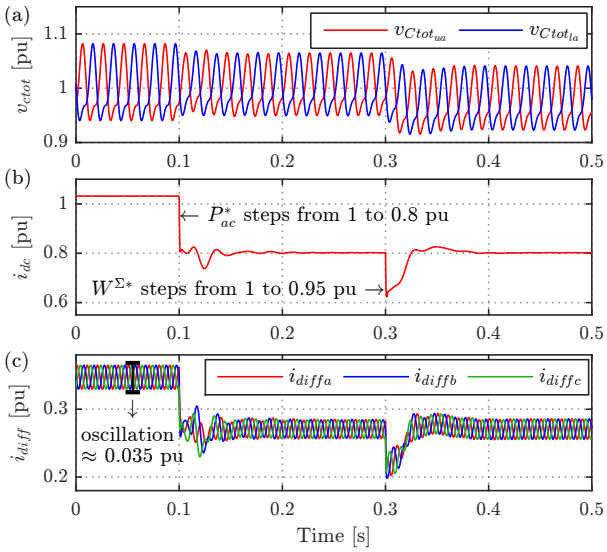


Fig. 6. Simulation results of Control Structure **a3**. (a) arm capacitor voltages $v_{Ctot_{ula}}$; (b) dc current $i_{dc}$; (c) differential current $i_{diff_j}$.

the reference of the RMS value of the ac component of the differential current $I^{ac*}_{diff_j}$:

$$I^{ac*}_{diff_j} = -\frac{\mathrm{PI}_{W^{\Delta}_j}\left(\overline{W}^{\Delta*}_j - \overline{W}^{\Delta}_j\right)}{2V_g} \tag{30}$$

Then, we need to generate the angles for the fundamental frequency components of the differential currents. The simplest way is to align $\varphi_j$ with the grid voltage phase angle, which is direct measurement by the PLL [13]. In this way:

$$i^{ac*}_{diff_j} = \mathbf{A} I^{ac*}_{diff_j} \tag{31}$$

$$\mathbf{A} = \sqrt{2}\begin{bmatrix} \cos(\omega_g t) & 0 & 0 \\ 0 & \cos(\omega_g t - \frac{2}{3}\pi) & 0 \\ 0 & 0 & \cos(\omega_g t + \frac{2}{3}\pi) \end{bmatrix}$$

Fig. 6 shows the simulation results of Control Structure **a3**. This control structure enables the MMC to operate with designed dynamics in both events, ac power reference changes at 0.1 s and stored energy changes at 0.3 s.

Note that the energy difference PI controller works independently in each leg. The generated current sum $\sum i^{ac*}_{diff_j}$ may be non-zero, which causes oscillations on the dc current during transient as shown in Fig 6(b). An additional transformation **K** can be used to force $\sum i^{ac*}_{diff_j}$ to be zero [12] [19]. The transformation modifies the angles generated for the fundamental frequency components of the differential currents, which also leads to a different gain in (30). The additional gain effect will

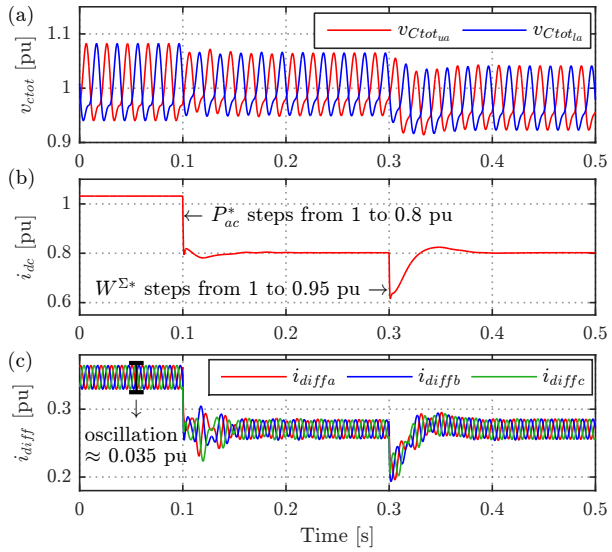


Fig. 7. Simulation results of the Control Structure **a3** with additional matrix transformation **K**. Dc current waveform is improved with less oscillation.

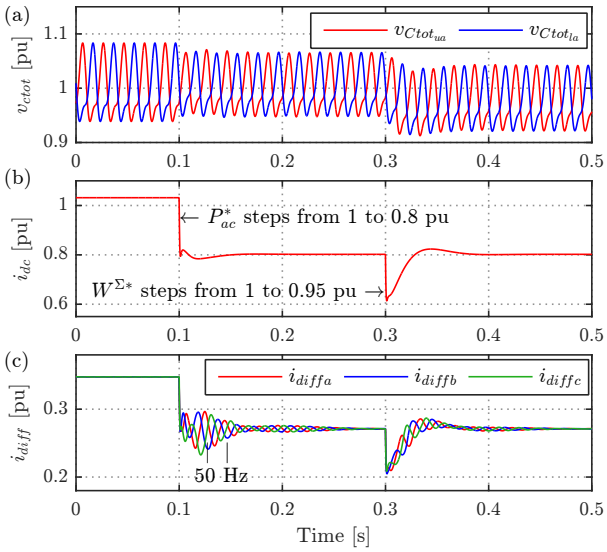


Fig. 8. Simulation results of Control Structure **b3**. (a) arm capacitor voltages $v_{Ctot_{ula}}$; (b) dc current $i_{dc}$; (c) differential current $i_{diff_j}$.

be compensated by the PI controller.

$$i^{ac*}_{diff_j} = \mathbf{K}\mathbf{A}I^{ac*}_{diff_j},\ \mathbf{K} = \begin{bmatrix} 1 & \frac{-1}{2} & \frac{-1}{2} \\ \frac{-1}{2} & 1 & \frac{-1}{2} \\ \frac{-1}{2} & \frac{-1}{2} & 1 \end{bmatrix} \tag{32}$$

With the matrix transformation, the dc current is clearly improved with less oscillation during transient in Fig. 7(b) compared to Fig. 6(b).

### D. CM and Vertical Energy Balancing Control (*b3*)

In the previous Control Structure **a3**, dc current is controlled by establishing a link of stored energy in the MMC with the dc and ac power. Ac components of the differential currents are introduced to balance the energy stored in the upper and lower arms. The ac components are generated in a way that the sum of them is always zero. However $2\omega_g$ oscillation on $i_{diff_j}$ in Fig. 7 can still be observed.

The oscillation can be slightly reduced with a high bandwidth PI controller. But a better solution is to use CM. With CM, the oscillation can be naturally eliminated without interfering the dc current. This leads to Control Structure **b3**, which is generally called *Energy Based Control* in the literature [13] [15] and [20].

This control structure allows a perfect decoupling between the internal MMC variables and has a full control of the energy distribution in the MMC arms. Compared to **a3**, the dynamics of the $i_{diff_j}$ controllers in **b3** are less demanding because no oscillation naturally appears, as shown in Fig.8.

During the transient, the differential current in Fig. 8 has a noticeable 50 Hz oscillation. This indeed proves that in the method **b3** the fundamental frequency component in the $i_{diff_j}$ is used to compensate the energy difference between the upper and lower arms.

### E. Conclusion on the control structures

UCM does not consider the oscillating components of $v_{Ctot_{uj}}$. This creates insertion index generation errors that in turn bring asymptotic stability to the system. However, it also generates the $-2\omega_g$ component of the differential current. Contrariwise, CM enables $v_{ulj}$ to follow exactly its reference $v^*_{ulj}$. By setting $(v^*_{uj} + v^*_{lj})$ equivalent to $v_{dc}$, in steady state, $i_{diff_j}$ is constant since $v_{diff_j}$ in the left part of (5) becomes zero. Then the $-2\omega_g$ component naturally disappears, the asymptotic stability of the MMC is lost simultaneously, so that energy sum and energy difference controls should be introduced in the control system.

## V. Experiments on a Small-Scale Test Bench

In this section, the control structures are tested on an experimental 21-level MMC prototype shown in Fig. 9(a). This prototype is connected to a 200 V, 50 Hz ac grid generated by a power amplifier, and a 400 V dc link generated by a dc source. Its maximum active power is $\pm 5$ kW. The detail parameters are provided in Table I.

### A. MMC prototype description

The MMC prototype is a scaled-down mock-up of the MMC used in the INELFE project [21]. For reliable studies of the ac/dc power interactions, the passive elements are sized by using the per-unit approach as follows:

1) The SM capacitors of the prototype is designed to preserve the same electrostatic constant of 40 ms as in practical projects.
2) Usually the MMC arm inductors are designed to limit the current boost during critical faults. In the prototype, however, this value is doubled in order to limit the output current ripples due to the reduction of SM levels. Because the energy stored in the inductors are negligible compared

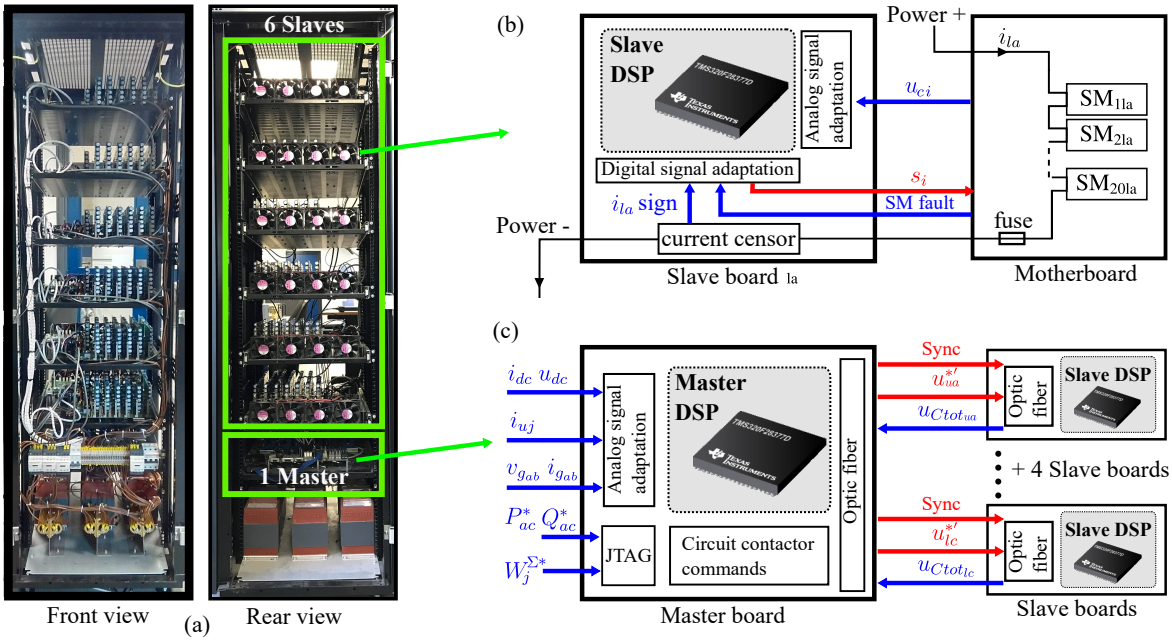


Fig. 9. (a) Front and rear views of the experimental MMC prototype (b) Arm level control (c) System level control

TABLE I
MMC PROTOTYPE PARAMETERS

| | | | |
|---|---|---|---|
| Nominal Power $P_{nom}$ | 5 kW | Arm inductance $L_{arm}$ | 10 mH |
| Dc bus voltage $V_{dc}$ | 400 V | Arm resistance $R_{arm}$ | 0.16 Ω |
| Ac line voltage $U_{ac}$ | 200 V | Transformer inductance $L_f$ | 5 mH |
| Number of SM $N_{sm}$ | 20 | Transformer resistance $R_f$ | 0.1 Ω |
| | | SM capacitance $C_{sm}$ | 8 mF |

to that in the SM capacitors, this choice of inductance value is justified.

The components of one submodule is shown in Fig. 10. Following the defined electrostatic inertia, the submodule capacitance is 8 mF. This is realized by parallel connection of eight capacitors of 1 mF. Some additional capacitors are added on the board to emulate an unbalance between the submodules and the arms. The MOSFET PSMN3R8-100BS allows a maximum voltage of 100 V, maximum current of 120 A and conduction resistance of 3.9 mΩ. Two gate drives are ACPL-332J with optical isolation between the power and control parts. An optically isolated voltage sensor ACPL-C87B is used for the measurement of submodule capacitor voltages.

The submodule board has no on-board controller. It is designed as a male card to be mounted on to its motherboard to receive external power supply and signals. The edge connector provides the gating signals to the gate drivers. In return, the measured capacitor voltage is transmitted through this connector to the motherboard. One motherboard accommodates 20 submodules. The assembly of one arm is shown in Fig. 11. For the sake of easy assembly and maintenance, the control system is installed in another board, called "slave control board".

The prototype is used for multi-research proposes so that its control architecture is accessible, reprogrammable and efficient. A distributed control system is proposed as shown in Fig.

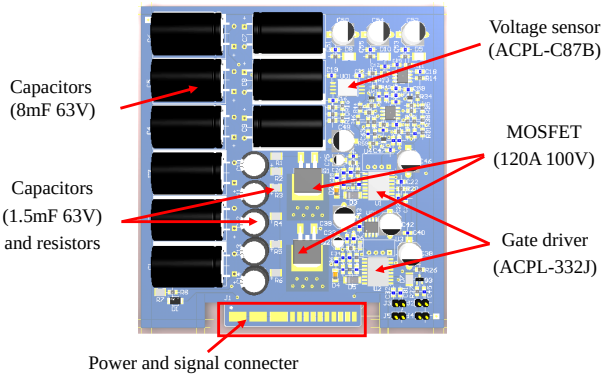


Fig. 10. Submodule board elements

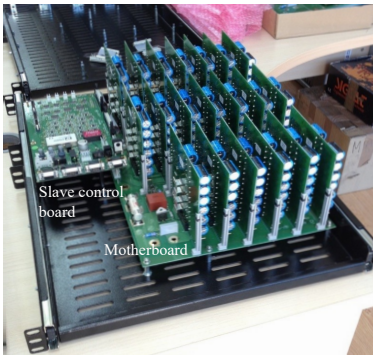


Fig. 11. Arm valve elements assembly

9(a). The control system contains 7 DSPs TMS320F28377D, featuring a "Master-Slave" configuration.

Six Slave DSPs for arm level control are distributed on the six arms and placed in the slave control board. The main tasks of the low level control is 1) to active a number of SMs to

TABLE II
RESPONDING TIME OF MMC PROTOTYPE CONTROLLERS

| | | | |
|---|---|---|---|
| Energy sum PI$_{W_j^{\Sigma}}$ | 50 ms | Differential current PI$_{i_{diff_j}}$ | 5 ms |
| Energy difference PI$_{W_j^{\Delta}}$ | 100 ms | Grid current PI$_{i_{g_{dq}}}$ | 1 ms |
| CCSC PI$^{-2\omega}_{i_{diff_j}}$ | 10 ms | | |

form the required arm reference voltage level, and 2) to keep the SM capacitor voltages staying in an acceptable range. The low level control adopts the algorithm introduced in [17].

This mechanism requires the SM capacitor voltages and the current direction. As mentioned in the submodule design part, the voltages are measured from the submodule board, collected in the motherboard and then passed to the Slave control board. The current direction is obtained by the current sensor in the Slave board as shown in Fig. 9(b). In general, the Slave DSP receives the arm voltage reference from the Master DSP, decides to switch off/on the specific overcharged/undercharged submodule depending the arm current direction. The sampling frequency of the low level control is 50 kHz.

One Master DSP is responsible for the system level control of the MMC. It can be easily programmed to run either control ctructures presented in Section IV. As shown in Fig. 9(c), the Master DSP deals with three kinds of signals:

1) analogue signals of current and voltage measurement from the main circuit;
2) digital signals of MMC arm equivalent capacitor voltage from the Slave DSP
3) digital signals of the MMC operating point reference and commands from the user.

In this manner, the Master DSP calculates the reference arm voltages and send them to the Slave DSPs via fibre optic cables. The sampling frequency of the system level control is 12.5 kHz.

To start/stop smoothly the prototype and for the sake of protection, buffer resistors, contactors and circuit breakers are inserted in the MMC prototype main circuit, as shown in Fig. 9(a). The command signals for the contactors are also sent by the Master DSP.

### *B. Experiment 1: active power reference variation in control structures **a1**, **a3** and **b3***

The first experiment shows the dc current evolution with a power reference $P^*_{ac}$ steps from 0 to 2.5 kW. Three Control Structures **a1**, **a3** and **b3** are tested. Control parameters are listed in Table II and test results are shown in Fig. 12.

Control Structure **a1** does not deal with the dc component of the differential current, so that the dc link current is poorly damped. As mentioned in Part IV-A, this can be solved by regulating the stored energy in the legs. Control Structures **a3** and **b3** lead to much better dc current response with less overshoot and higher damping effect. The results of **a3** and **b3** are highly coherent, with negligible difference caused by the down-scaling effect since that only 20 SM per arm are

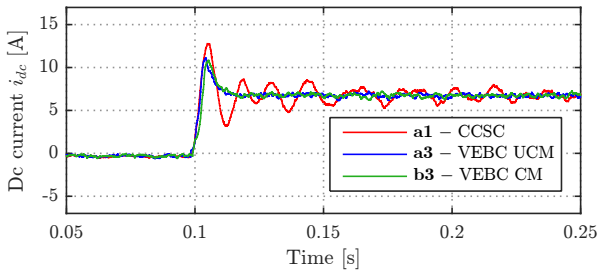


Fig. 12. Experimental results: $i_{dc}$ with $P^*_{ac}$ increases from 0 to 0.5 pu.

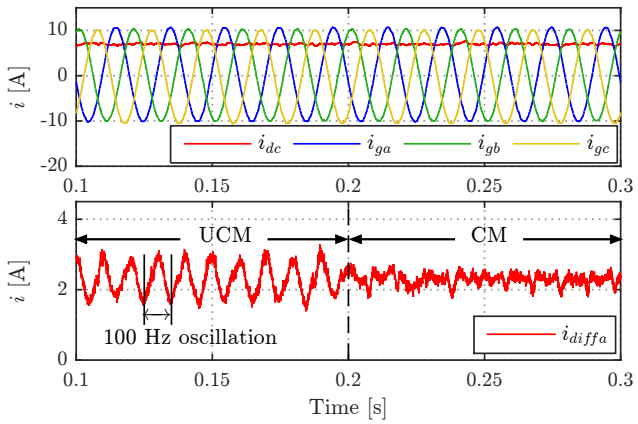


Fig. 13. Experimental results : 100 Hz oscillation of the differential current is eliminated with CM.

used. This confirms that the modulation methods do not have impact on the dc component of the differential currents. Its impact on the $-2\omega_g$ component of the differential current is confirmed in the next experiment.

### *C. Experiment 2: comparison of modulation methods with control structures **a3** and **b3***

This second experiment is proposed to verify the impact of CM and UCM on the $-2\omega_g$ oscillation of the differential current. As stated in Section IV, UCM gives rise to 100 Hz oscillations that naturally disappears in CM.

Both Control Structures **a3** and **b3** are implemented in the Master DSP with the controllers using the same parameters listed in Table II. The MMC is initially controlled with **a3** and operates at 2.5 kW. The control system is switched to **b3** at 0.2 s. As shown in Fig. 13, the 100 Hz oscillation is eliminated after the CM is applied. It is noticed that this transition does not influence the dc current, because ac components of the differential currents only circulate internally in the converter. Their sum is always kept to zero, thus no dc component is superimposed to the dc current. This reconfirm the results obtained in the first experiment.

### *D. Experiment 3: energy reference variation in control structure **b3***

The last experiment is to show the dc current variation following an energy reference decrease in Control Structure **b3**. At 0.82 s, the average energy sum reference $\overline{W}_j^{\Sigma *}$ steps

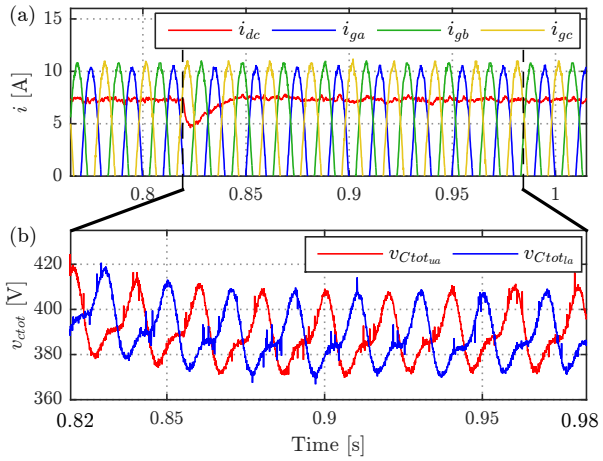


Fig. 14. Transient waveforms when $W_j^{\Sigma*}$ steps from 1.0 pu to 0.95 pu at 0.82 s: (a) $i_{dc}$ sags then recovers (b) $v_{Ctot}$ decreases from 400 V to 390 V.

from 1 pu to 0.95 pu. This step induces a transient on the dc current as shown in Fig. 14. The result corresponds to the simulation result shown in Fig. 8(a). Because the system is decoupled, the ac side currents are not impacted by the step of energy sum reference. Fig. 14(b) shows the evolution of the equivalent arm capacitor voltages after the step of the energy sum reference. The voltages drop from an average value of 400 V to 390 V, corresponding to 0.05 pu reduction of the energy sum.

## VI. Conclusion

This paper gives a comprehensive description of the MMC's control structures. A Non-Energy Based Control, such as CCSCdq, depends on the UCM to guarantee its stability. The system is usually poorly damped. UCM also give rise to the appearance of $-2\omega_g$ oscillations on the differential current. With the physical meaning of each system variable explained, a full Energy based control is progressively introduced. The system can be controlled with desired dynamics and the $-2\omega_g$ oscillation on the differential current no longer exists.

The performance of the Full Energy Based Control and the difference between UCM and CM are verified experimentally. The experiments are carried out on a small-scale grid connected 21-level MMC prototype. The obtained results confirmed the behaviour issued from simulations Tests of these control structures under unbalanced grid condition will be carried out in the future.

## References


[1] A. Lesnicar and R. Marquardt, "An innovative modular multilevel converter topology suitable for a wide power range," in *2003 IEEE Bologna Power Tech Conference Proceedings,*, vol. 3. IEEE, 2003, pp. 6–pp.

[2] T. Westerweller, K. Friedrich, U. Armonies, A. Orini, D. Parquet, and S. Wehn, "Trans bay cable – world's first hvdc system using multilevel voltage-sourced converter," *Proc. 2010 CIGRE, Paris*, 2010.

[3] K. Ilves, A. Antonopoulos, S. Norrga, and H.-P. Nee, "Steady-state analysis of interaction between harmonic components of arm and line quantities of modular multilevel converters," *IEEE Transactions on Power Electronics*, vol. 27, no. 1, pp. 57–68, jan 2012.

[4] L. Harnefors, A. Antonopoulos, S. Norrga, L. Angquist, and H.-P. Nee, "Dynamic analysis of modular multilevel converters," *IEEE Transactions on Industrial Electronics*, vol. 60, no. 7, pp. 2526–2537, 2013.

[5] A. Antonopoulos, L. Angquist, L. Harnefors, K. Ilves, and H.-P. Nee, "Global asymptotic stability of modular multilevel converters," *IEEE Transactions on Industrial Electronics*, vol. 61, no. 2, pp. 603–612, feb 2014.

[6] Z. Li, P. Wang, Z. Chu, H. Zhu, Y. Luo, and Y. Li, "An inner current suppressing method for modular multilevel converters," *IEEE Transactions on Power Electronics*, vol. 28, no. 11, pp. 4873–4879, 2013.

[7] Q. Tu, Z. Xu, and J. Zhang, "Circulating current suppressing controller in modular multilevel converter," in *IECON 2010 - 36th Annual Conference on IEEE Industrial Electronics Society*. IEEE, nov 2010.

[8] A. Jamshidifar and D. Jovcic, "Small-signal dynamic dq model of modular multilevel converter for system studies," *IEEE Transactions on Power Delivery*, vol. 31, no. 1, pp. 191–199, 2015.

[9] T. Li, A. M. Gole, and C. Zhao, "Harmonic instability in mmc-hvdc converters resulting from internal dynamics," *IEEE Transactions on Power Delivery*, vol. 31, no. 4, pp. 1738–1747, 2016.

[10] J. Freytes, G. Bergna, J. A. Suul, S. D'Arco, F. Gruson, F. Colas, H. Saad, and X. Guillaud, "Improving small-signal stability of an mmc with ccsc by control of the internally stored energy," *IEEE Transactions on Power Delivery*, vol. 33, no. 1, pp. 429–439, 2018.

[11] A. Antonopoulos, L. Angquist, and H.-P. Nee, "On dynamics and voltage control of the modular multilevel converter," in *Power Electronics and Applications, 2009. EPE'09. 13th European Conference on*. IEEE, 2009, pp. 1–10.

[12] P. Münch, D. Görges, M. Izák, and S. Liu, "Integrated current control, energy control and energy balancing of modular multilevel converters," in *IECON 2010-36th Annual Conference on IEEE Industrial Electronics Society*. IEEE, 2010, pp. 150–155.

[13] P. Delarue, F. Gruson, and X. Guillaud, "Energetic macroscopic representation and inversion based control of a modular multilevel converter," in *Power Electronics and Applications (EPE), 2013 15th European Conference on*. IEEE, 2013, pp. 1–10.

[14] G. Bergna, E. Berne, P. Egrot, P. Lefranc, A. Arzande, J.-C. Vannier, and M. Molinas, "An energy-based controller for hvdc modular multilevel converter in decoupled double synchronous reference frame for voltage oscillation reduction," *IEEE Transactions on Industrial Electronics*, vol. 60, no. 6, pp. 2360–2371, 2013.

[15] S. Samimi, F. Gruson, P. Delarue, F. Colas, M. M. Belhaouane, and X. Guillaud, "Mmc stored energy participation to the dc bus voltage control in an hvdc link," *IEEE Transactions on Power Delivery*, vol. 31, no. 4, pp. 1710–1718, 2016.

[16] J. Freytes, G. Bergna, J. Suul, S. D'Arco, H. Saad, and X. Guillaud, "Small-signal model analysis of droop-controlled modular multilevel converters with circulating current suppressing controller," 2017.

[17] Q. Tu, Z. Xu, and L. Xu, "Reduced switching-frequency modulation and circulating current suppression for modular multilevel converters," *IEEE transactions on power delivery*, vol. 26, no. 3, pp. 2009–2017, 2011.

[18] A. Ferreira, C. Collados, O. Gomis-Bellmunt, and M. Teixido, "Modular multilevel converter electrical circuit model for hvdc applications," in *2015 17th European Conference on Power Electronics and Applications (EPE'15 ECCE-Europe)*. IEEE, 2015, pp. 1–10.

[19] K. Shinoda, J. Freytes, A. Benchaib, J. Dai, H. Saad, and X. Guillaud, "Energy difference controllers for mmc without dc current perturbations," in *The 2nd International Conference on HVDC (HVDC2016)*, 2016.

[20] J. Freytes, G. Bergna, J. A. Suul, S. D'Arco, H. Saad, and X. Guillaud, "State-space modelling with steady-state time invariant representation of energy based controllers for modular multilevel converters," in *2017 IEEE Manchester PowerTech*. IEEE, 2017, pp. 1–7.

[21] P. L. Francos, S. S. Verdugo, H. F. Álvarez, S. Guyomarch, and J. Loncle, "Inelfe — europe's first integrated onshore hvdc interconnection," in *2012 IEEE power and energy society general meeting*. IEEE, 2012, pp. 1–8.

**Haibo Zhang** was born in Shanghai, China, in 1990. He received the Ph.D degree in electrical engineering from Université des Sciences et Technologies de Lille, France. Since 2018, he has been a Research Engineer in the Laboratoire d'Electrotechnique et d'Electronique de Puissance of Lille (L2EP), France. His research interests include modeling and control of power electronic converters in transmission system and hardware-in-the loop simulation.

**Mohamed Moez Belhaouane** received the master's degree in automatic control and the Ph.D. degree in electrical engineering from Ecole Supérieure des Sciences et Techniques de Tunis and Polytechnic School of Tunisia, in 2005 and 2011, respectively. He is currently a Senior Research Engineer in L2EP Laboratory (Laboratoire d'Electrotechnique et d'Electronique de Puissance) at Ecole Centrale de Lille, France. Prior to joining the Electric Grid Research Team in L2EP Laboratory, he was an Associate Professor in Ecole Nationale Superieure d'Ingénieurs de Tunis. Earlier, he was also an Assistant Professor at Ecole Nationale d'Ingénieurs de Gabès. His main research interests include the modeling, analysis and control issues based on the high integration of power electronics in high-voltage power transmission systems. Moreover, his research advances involve also the development and implementation of advanced control strategies using hardware-in-the-loop and power-hardware-in-the-loop concepts based on small-scale mock-up.

**Frédéric Colas** was born in Lille, France, in 1980. He received his Ph.D. degree in control systems from Ecole Centrale de Lille, Lille, in 2007. He is a member of the Laboratory of Electrical Engineering (L2EP), Lille, and a Research Engineer at Arts et Metiers Institute of Technology. His research interests include the integration of dispersed generation systems in electrical grids, advanced control techniques for power systems, and hardware-in-the-loop simulation.

**Riad Kadri** was born in Setif, Algeria, in 1979. He received the M.S. degree in electrical engineering from the University of Setif, Algeria, in 2006, and the Ph.D. degree in electrical engineering from the University of Poitiers, Poitiers, France, in 2010. Between 2009 and 2011, he became a temporary Assistant Professor at the Department of Electrical and Electronics Engineering, University Institute of Technology of Poitiers, France. He is currently a Research Engineer with the Electrical Engineering and Power Electronics Laboratory (L2EP), Lille, France. His main research interests include analysis, real time simulation, and design of power converters for renewable energy sources and electrical network.

**François Gruson** received the Ph.D. degree in electrical engineering from the Ecole Centrale de Lille, Lille, in 2010. Since 2011, he has been working as Associate Professor at Arts et Metiers Institute of Technology in the Laboratoire d'Electrotechnique et d'Electronique de Puissance of Lille (L2EP), Lille, France. His research interests include power electronic converter and power quality for distribution and transmission grid application and especially for HVDC transmission grid.

**Xavier Guillaud** (M'04) joined the Laboratory of Electrical Engineering and Power Electronics (L2EP), Lille, in 1993. He has been professor with Ecole Centrale de Lille since 2002. First, he worked on the modeling and control of power electronic systems. Then, he studied the integration of distributed generation and especially renewable energy in power systems. Nowadays, he is studying the high voltage power electronic converters in transmission system. He is leading the development of an experimental facility composed of actual power electronic converters interacting with virtual grids modeled in real-time simulator. He is involved on several projects about power electronic on the grid within European projects and different projects with French companies. He is member of the Technical Program Committee of Power System Computation Conference (PSCC) and associated editor of Sustainable Energy, Grids and Networks (SEGAN).